arXiv:1103.4026v1 [astro-ph.GA] 21 Mar 2011

Using Hα Morphology and Surface Brightness Fluctuations to Age-Date Star Clusters in M83

Bradley C. Whitmore,[1] Rupali Chandar,[2] Hwihyun Kim,[3] Catherine Kaleida,[3] Max Mutchler,[1] Daniela Calzetti,[4] Abhijit Saha,[5] Robert O'Connell,[6] Bruce Balick,[7] Howard E. Bond,[1] Marcella Carollo,[8] Michael J. Disney,[9] Michael A. Dopita,[10] Jay A. Frogel,[11] Donald N. B. Hall,[12] Jon A. Holtzman,[13] Randy A. Kimble,[14] Patrick J. McCarthy,[15] Francesco Paresce,[16] Joseph I. Silk,[17] John T. Trauger,[18] Alistair R. Walker,[19] Rogier A. Windhorst,[3] and Erick T. Young[20]

whitmore@stsci.edu

[1]Space Telescope Science Institute, Baltimore, MD, USA

[2]Department of Physics & Astronomy, The University of Toledo, Toledo, OH 43606

[3]School of Earth and Space Exploration, Arizona State University, Tempe, AZ 85287-1404, USA

[4]Department of Astronomy, University of Massachusetts, Amherst, MA 01003, USA

[5]NOAO, Tucson, AZ 85726-6732, USA

[6]Department of Astronomy, University of Virginia, Charlottesville, VA 22904-4325, USA

[7]Department of Astronomy, University of Washington, Seattle, WA 98195-1580, USA

[8]Institute of Astronomy, ETH-Zurich, Zurich, 8093 Switzerland

[9]Department of Physics and Astronomy, Cardiff University, Cardiff CF24 3AA, UK

[10]Research School of Astronomy & Astrophysics, The Australian National University, Cotter Road, Weston Creek, ACT 2611, Australia

[11]AURA, Washington, DC 20005, USA

[12]Institute for Astronomy, Honolulu, HI 96822, USA

[13]New Mexico State University, Las Cruces, NM 88003, USA

[14]Goddard Space Flight Center, Greenbelt, MD 20771, USA

[15]Carnegie Institute of Washington, Pasadena, CA 91101-1292, USA

[16]Istituto di Astrofisica Spaziale e Fisica Cosmica, INAF, Via Gobetti 101, 40129, Bologna, Italy

[17]Department of Physics, University of Oxford, Oxford OX1 3PU, UK

[18]NASA JPL, Pasadena, CA 91109, USA

[19]Cerro Tololo Inter-American Observatory, La Serena, Chile

[20]NASA–Ames Research Center, Moffett Field, CA 94035, USA

ABSTRACT

We use new WFC3 observations of the nearby grand design spiral galaxy M83 to develop two independent methods for estimating the ages of young star clusters. The first method uses the physical extent and morphology of Hα emission to estimate the ages of clusters younger than $\tau \approx 10$ Myr. It is based on the simple premise that the gas in very young ($\tau <$ few Myr) clusters is largely coincident with the cluster stars, is in a small, ring-like structure surrounding the stars in slightly older clusters since massive star winds and supernovae have had time to push out the natal gas (e.g., $\tau \approx 5$ Myr), and is in a larger ring-like bubble for still older clusters (i.e., $\approx$ 5–10 Myr). If no Hα is associated with a cluster it is older than ≈ 10 Myr. The second method is based on an observed relation between pixel-to-pixel flux variations within clusters and their ages. This method relies on the fact that the brightest individual stars in a cluster are most prominent at ages around 10 Myr, and fall below the detection limit (i.e., $M_V < -3.5$) for ages older than about 100 Myr. Older clusters therefore have a smoother appearance and smaller pixel-to-pixel variations. The youngest clusters also have lower flux variations, hence the relationship is double valued. This degeneracy in age can be broken using other age indicators such as Hα morphology. These two methods are the basis for a new morphological classification system which can be used to estimate the ages of star clusters based on their appearance. We compare previous age estimates of clusters in M83 determined from fitting *UBVI*Hα measurements using predictions from stellar evolutionary models with our new morphological categories and find good agreement at the $\approx 95\%$ level. The scatter within categories is ≈ 0.1 dex in $\log \tau$ for young clusters (<10 Myr) and ≈ 0.5 dex for older (>10 Myr) clusters. A by-product of this study is the identification of 22 "single-star" HII regions in M83, with central stars having ages ≈ 4 Myr.

Subject headings: galaxies: individual (M83) — galaxies: star clusters: general — HII regions — ISM: bubbles — stars: formation

1. Introduction

Age estimates are required for studying the evolutionary history of star clusters. Based on such age estimates, a general framework has been developed starting from formation within the dense cores of giant molecular clouds (GMCs); a stage where the young stars are

completely obscured by their dusty gas cocoons; an emerging stage where the clusters become visible in the infrared (IR) and then visible in the optical as stellar winds and supernovae blow away the gas and dust; a stage where an expanding bubble of ionized gas is blown; and later stages with no evidence of ionized gas (e.g., see the Lada & Lada 2003 review article).

In the past, two general methods for estimating the ages of unresolved extragalactic star clusters have been used. The first requires obtaining high quality spectroscopic observations covering wavelength regions of lines which change as a function of time. Examples of this approach include Bica & Alloin (1986), Schweizer & Seitzer (1993), Whitmore et al. (1999), Bastian et al. (2009) and Wofford et al. (2010). While these spectroscopic observations typically provide high quality age determinations, they are limited to age-dating relatively small numbers of bright clusters due to constraints on the brightness of clusters that can be observed spectroscopically in a reasonable amount of time. The standard method for age-dating large numbers of extra-galactic clusters compares photometry in several broadband filters (e.g., *UBVI*) with predictions from population synthesis models (e.g., Chandar et al. 2010).

Comparisons of age estimates using spectroscopic and photometric observations of the same clusters show good agreement in most cases. An early example of this is the famous Searle et al. (1980) paper where they compare integrated four-filter *ugvr* photometry of 61 star clusters in the Magellanic Clouds with the strength of different spectral features (e.g., Balmer lines, *G* band, etc.) A recent example is Wofford et al. (2010) who compared ages estimated from spectral energy distribution (SED) fitting with those derived from UV spectroscopy for 14 young ($\tau \lesssim 30$ Myr) clusters in the nuclear starburst region of M83 and found that the photometric ages are within a factor of 1.4 of the spectroscopic ones. Whitmore et al. (2010) find similar agreement between their photometric age estimates and the spectroscopic estimates from Bastian et al. (2009) for clusters in the Antennae galaxies. While generally satisfactory, both the spectroscopic and photometric techniques have limitations. It is therefore important to develop independent methods for estimating the ages of clusters, especially for cases where spectroscopic or multi-band photometric observations are not available and it is necessary to estimate ages based on morphological appearance alone.

Here, we develop two new methods for estimating the ages of young star clusters in nearby galaxies based on high-resolution images at optical wavelengths. The first method uses the morphology of the ionized gas and its position relative to the cluster stars, as measured from narrowband Hα emission, to estimate ages (τ) for clusters younger than $\tau \lesssim 10$ Myr. This method relies on the general premise that the distribution of Hα will be largely coincident with the distribution of optical light in the youngest clusters (i.e., $<$ few

Myr), will be in a small ring-like structure around the optical stellar emission in slightly older clusters where massive star winds and supernovae have had time to blow a bubble (i.e., $5 \approx$ Myr), and will be in a larger ring-like bubble for still older clusters (i.e., 5–10 Myr).

Many past observational and theoretical studies of HII regions and "supershells" in the Milky Way and nearby galaxies have laid the groundwork for this method. For example, Walborn (2002; see also Walborn & Parker 1992 and especially Walborn 2010 for related discussions) outlined an evolutionary cluster sequence based on observed properties of several well known clusters and OB associations in the Milky Way with ages ranging from ≈ 1 Myr to ≈ 10 Myr. This sequence was then used to illustrate observed changes with age in the visually brightest stars, in the ionized gas and dust content, and in the existence of red supergiants. Much of this sequence was based on spectroscopy of individual stars. While we are unable to make similarly detailed observations at the distance of M83, many of the same basic correlations and underlying physical processes are relevant for the age sequence outlined in this paper. Theoretically, several works have made predictions for the size evolution of an expanding HII region over time. Oey & Clark (1997, 1998) model the size evolution due to mass loss and supernova-injected energy from cluster stars, and assume that expanding bubbles "stall" when their internal pressure equals the ambient pressure in the ISM. These simulations predict a strong dependence of bubble size on both the age and mass of the central cluster. (e.g., Weaver et al. 1977, Oey & Massey 1995, Oey & Garcia-Segura 2004, Dopita et al. 2006a, 2006b). Our observations of clusters in M83 reveal a strong dependence of bubble size on cluster age, and possibly a weak dependence on cluster mass, as discussed in Section 6.

The second method developed in this paper uses the surface brightness fluctuations of cluster stars to estimate their ages. Young clusters have strong pixel-to-pixel flux variations, due to the presence of massive, luminous stars. As a cluster ages, the bright, short-lived massive stars disappear, and these fluctuations fade in strength. This technique is especially useful in the range $\tau \approx$ 10–100 Myr, ages that can be somewhat difficult to deal with using the SED method, because the predicted integrated colors loop back on themselves.

Our primary target for this study is the spiral galaxy M83. At a distance of 4.5 Mpc (corresponding to a distance modulus of $m - M = 28.28$; Thim et al. 2003, and a pixel scale of 0.876 pc pixel^{-1}), M83, nicknamed the "Southern Pinwheel," is the nearest massive grand-design spiral galaxy. It is a slightly barred galaxy, with a Hubble type SAB(s)c (3RC). In this work, we make use of observations taken with the Wide-Field Camera 3 (WFC3), which were described in detail in Dopita et al. (2010) and Chandar et al. (2010). Briefly, the observations are part of the Early Release Science project 1 (ERS1) program 11360 (PI: O'Connell) and were taken in August, 2009. Observations were taken in several broadband

("UV" - F225W, "U" - F336W, "B" - F438W, "V" - F555W, "I" - F814W, "J" - F110W, and "H" - F160W), and narrowband filters ([OIII] - F373N, Hβ - F487N, [OII] F502N, Hα - F657N, [SII] - F673N, Paschenβ - F128N, and [FeII] - F164N). In the Appendix we briefly investigate clusters in M51 and find that the age versus morphological category relationship derived for M83 is appropriate for this galaxy as well.

This paper is organized as follows: In Section 2 we outline our working scheme for an evolutionary cluster classification system based on observables at optical wavelengths. In Section 3 we investigate the correlation between Hα morphology and SED age estimates while Section 4 examines the correlation between the strength of surface brightness fluctuations within clusters and their ages. A catalog of smaller HII regions, apparently ionized by "single stars," is presented in Section 5. We examine the effect of cluster mass on Hα bubble size in Section 6, and summarize our primary results in Section 7.

2. An Evolutionary Classification Scheme Based on Observables at Optical Wavelengths

The early formative stages of star cluster evolution are best studied in the IR or microwave part of the spectrum, since the stars remain embedded in their placental dust cocoons for the first million years or so (Lada & Lada 2003). For example, in nearby groups and clusters in the Milky Way, individual young stellar objects (YSOs) can be age-dated using a classification scheme ranging from category 0 to III, as developed by Wilking et al. (1989) and Andre et al. (1993), based on near-IR observations.

In this paper we outline a working classification scheme for cluster evolution in external galaxies. We focus on the later stages based on the optical portion of the spectrum. Our primary goals are to test how well we can use Hα morphology and surface brightness fluctuations to age date star clusters. The basic categories are defined below. In all cases we assume that the clusters have radial profiles that are broader than the point-spread function (PSF), hence confusion with individual stars is not a major issue (see Chandar et al. 2010). Examples of clusters in categories 3 through 6 are shown in Figure 1. M83 clusters in categories 1 and 2 will be discussed in a later paper which presents our WFC3 observations in the J and H bands.

Category 1: **opaque dust cloud** - core of a GMC - dark region on optical image with no associated IR/UVIS source - often studied using millimeter observations of the HCN line (e.g., Gao & Solomon 2004)

Category 2a: - **embedded cluster** - weak IR source with no optical (I band) counterpart (i.e., Av $>$ 10) - no ionized Hα gas visible

Category 2b: - **obscured cluster** - strong IR and weak optical source (3 $<$ Av $<$ 10)

Category 3: - **emerging cluster** - ionized gas spatially coincident with cluster stars - cluster has a reddish color due to dust - surface brightness fluctuations from individual stars are relatively small since the brightest, evolved stars have not yet appeared

Category 4a: - **very young cluster** - ionized gas in a small bubble surrounding the cluster - cluster has a bluish color since most of the dust has been expelled - surface brightness fluctuations from individual stars are strong

Category 4b: - **young cluster** - similar to category 4a but the ionized gas is now in a large bubble surrounding the cluster (i.e., radii larger than approximately 20 pc) - surface brightness fluctuations from individual stars reach maximum

Category 5a: - **young/intermediate-age cluster** - no ionized gas is observed - surface brightness fluctuations are still present, but weaker

Category 5b: - **intermediate-age cluster** - ionized gas and surface brightness fluctuations among cluster stars are not observed - cluster has a slightly redder color due to aging of stars

Category 6: - **old cluster** - no ionized gas or surface brightness fluctuations among cluster stars are observed, - cluster appears yellow/red with no evidence of dust in vicinity

3. Hα Morphology as an Age Indicator for $\tau \lesssim$ 10 Myr Clusters

3.1. General Trends

In principle, it should be possible to approximately estimate the ages of young ($\tau \lesssim$ 10 Myr) star clusters from the size of the ionized gas (Hα) bubble that surrounds them, as outlined in Sections 1 and 2. In this section we test this idea by selecting a representative catalog of young clusters primarily based on their apprearance in the narrowband Hα image (i.e., the red color in Figure 2), and then visually classify each source based on the scheme outlined in Section 2. Each region is then matched with the apparent central source of ionization from the Chandar et al. (2010) catalog, and compared with the ages from that paper based on SED fitting of the *UBVI*Hα bands. We do not, at this point, separate the

clusters by mass (the effect of cluster mass on bubble size is discussed in Section 6). Basic properties of the selected clusters are presented in Table 1, including position (RA and decl.) and photometric measurements (M_V, $V-I$, and $U-B$) for the central cluster.

The top row of Figure 1 shows examples of clusters in categories 3-6, with different Hα morphologies as outlined in Section 2. The bottom set of panels shows the location of each cluster in the category in a $V-I$ versus $U-B$ two-color diagram, where the photometry is drawn from the catalog described in Chandar et al. (2010). These panels show how well our morphological categories group the clusters in color-color space. Predictions from single stellar population G. Bruzual & S. Charlot (2009; private communications, hereafter BC09) models are superposed for comparison. As expected, clusters in the two youngest categories (3 and 4a) have somewhat higher extinction than those in later categories, which results in their colors spreading out along the reddening vector.

The middle set of panels present histograms of ages determined from the photometric dating method used in Chandar et al. (2010), for all clusters within a given category. These age estimates are included in Table 1. There is a clear trend for clusters in later categories to have older ages. For clusters with associated Hα emission, i.e., categories 3, 4a, 4b, we find an rms scatter of approximately 0.1 in $\log(\tau/\mathrm{yr})$ within each category. While our SED dating method includes photometry in the narrowband filter directly in the fit, the photometry is measured in a small (3 pixel radius) aperture that misses most or all of the Hα emission after Category 3. Hence the age estimates from the SED fitting and from the Hα morphology are largely independent of one another. The rms scatter in photometric ages for clusters identified within morphological categories 5 and 6 increases to ≈ 0.5 in $\log(\tau/\mathrm{yr})$, primarily because morphology becomes a cruder estimate in this age regime.

The good overall correlation between morphological classification and photometric age estimates from Chandar et al. (2010) is also apparent in Figure 2. This figure includes the SED ages for the clusters where morphological classifications have been determined using the prescripts defined in Section 2. The region covers a 1.0×1.0 kpc^2 area of M83. We note in particular the intermediate-age and old clusters in the upper central part of the image which have a fuzzy appearance due to the absence of bright young stars. The Appendix shows similar figures for selected regions in M51.

Figure 3 plots the morphological category assigned here versus $\log(\tau/\mathrm{yr})$ based on the SED age estimates from Chandar et al. (2010). The top panel shows the full range of cluster ages and categories. There is a clear, albeit nonlinear, correlation, with a steeper correlation between morphological category and age for clusters younger than $\approx 10^7$ yr. The nonlinearity is to be expected since Hα morphology evolves rapidly between the ages of 1–10 Myr. Note that in Figure 3 we have subdivided the morphological types into a finer grid of categories

(based on subjective estimates of the Hα bubble size) than outlined in Section 2. The bottom panel of Figure 3 shows one of the main results of this work, *that between 2 and 10 Myr, the clusters in M83 show a strong correlation between their Hα morphology and age.* This suggests that the morphology of ionized gas alone can be used as an age indicator. The best linear fit, shown in the figure, is given by: $MC = (3.04 \pm 0.32) \times \log(\tau/\mathrm{yr}) - 16.27 \pm 2.16$ (i.e., a 9 σ correlation) for $\log(\tau/\mathrm{yr}) < 7$, where MC is the morphological category defined in Section 2. This relationship is only relevant when Hα is present (i.e., categories 3 and 4). A similar, flatter, and less well-defined relationship exists for category 5 and higher, as shown in the top figure: $MC = (0.45 \pm 0.09) \times \log(\tau/\mathrm{yr}) + 1.78 \pm 0.82$ (i.e., a 5 σ correlation) for $\log(\tau/\mathrm{yr}) > 7$.

We note that a similar correlation exists between our morphological categories and ages estimated by comparing color magnitude diagrams of individual stars with stellar tracks for stars around some of our objects, as will be discussed in a study of 50 regions in M83 by H. Kim et al. (2011, in preparation).

While the dispersion in the estimated SED ages within each morphological category is remarkably small (see Figure 1 and Table 2), a close inspection reveals four outliers in category 5b. Three of these clusters (44034, 18032 and 74692) have no associated Hα emission, have relatively small pixel-to-pixel flux variations (discussed in Section 4), and have optical colors consistent with those predicted for extinction-free intermediate age clusters, and therefore almost certainly have ages $\log(\tau/\mathrm{yr}) \approx 8$. The SED fitting, however, erroneously assigned them lower ages ($\log(\tau/\mathrm{yr}) < 7$), and higher extinctions (i.e., $E(B{-}V) = 0.28$, 0.36, 0.50 mag). The fourth cluster (10114) has significantly bluer colors than the other clusters in category 5b. In retrospect, this cluster probably belongs in morphological category 4a, since there does appear to be a small amount of Hα emission associated with it. In this case it is the morphological classification which appears to be in error rather than the SED age estimate (the latter is $\log(\tau/\mathrm{yr}) = 6.6$). Overall, we find good agreement between the previously determined SED age and currently determined morphological category for 95% of the clusters (i.e., 84 out of 88 cases), demonstrating that *both* techniques are quite reliable.

3.2. An Empirical Correlation Between Hα Bubble Size and Cluster Age

While the good correlation between the morphological category and SED age found in Figure 3 is encouraging, this approach has several limitations. In particular, placing the clusters into the different categories is subjective and hence not easily automated. An additional complication is that an isolated, full 360 degree ring with a single dominant central cluster is very rare. Partial rings, multiple loops, and multiple clusters in the region are more

typical situations.[1]

Here, we attempt to better quantify the relationship between Hα morphology and cluster age by measuring the radii of the most prominent "coherent" ring or partial shell of ionized gas associated with the cluster stars. While the measurement of Hα bubble size is also difficult to automate, this more quantitative approach provides the opportunity for improving the correlation still further, and for exploring the impact that other physical parameters (e.g., cluster mass) have on this relationship.

Figure 4 plots the measured Hα bubble size versus photometric age for clusters younger than $\approx$ 10 Myr (top panel), and bubble size versus morphological category (bottom panel). There is clearly a strong correlation which suggests that Hα morphology alone can be used as an age indicator for clusters younger than $\approx$ 10 Myr. This figure hints at other intriguing results as well. The correlation between age and bubble size is strongest for clusters younger than $\log(\tau/\mathrm{yr}) \approx 6.7$, with typical bubbles growing from a few pc to $\approx$ 20 pc in size. After this time, between ages $\log(\tau/\mathrm{yr}) \approx 6.7$–6.9, there is a large range observed in bubble size, from $\approx$ 20 pc to nearly 80 pc, and no strong dependence on age. These trends are illustrated by the solid lines, which represent simple linear fits to observations in the two different regimes. The best linear fits for the top panel are given by: $\log(\tau/\mathrm{yr}) = (0.015\pm0.002)\times R(pc)+6.46\pm0.03$ for R $<$ 20 pc, and $\log(\tau/\mathrm{yr}) = (0.0014 \pm 0.0011) \times R(pc) + 4.37 \pm 0.22$ for R $>$ 20 pc. Similar fits are shown in the bottom panel, but numerical values are not included here since the use of morphological category makes them more qualitative. The large, open circles in the top panel of Figure 4 show the clusters with $M < 1 \times 10^4\ M_\odot$ and $\log(\tau/\mathrm{yr}) > 6.7$. These will be discussed further in Section 6.

4. Surface Brightness Fluctuations as Age Indicators for $\tau \lesssim$ 100 Myr Clusters

As discussed in Section 2, bright individual stars are expected to be visible within M83 clusters at ages younger than $\approx$ 100 Myr, giving the clusters a mottled appearance with relatively large pixel-to-pixel flux variations. After this, the flux variations have mostly disappeared, leading to a more uniform appearance among cluster stars. Compare, for example, the images in categories 4b and 5a in the top panel of Figure 1, where a number

[1]We note that the term "central" cluster may be misleading in some cases. There are many cases where the ring or shell is asymmetric, typically offset to the side where there is a more prominent dust lane. Examples of this morphology for super shells in the Antennae galaxy and a discussion in terms of the "blister" model of Israel (1978) are provided in Whitmore et al. (2010).

of bright individual cluster stars are clearly visible, with the images for categories 5b and 6, where individual cluster stars are no longer observed. Figure 2 also shows a variety of cases where older clusters appear as fuzzy objects while single individual stars are clearly observed within the young clusters.

Here, we use the strength of these surface brightness fluctuations to develop a new method for estimating the ages of clusters in M83. This is reminiscent of the surface brightness fluctuation method used to estimate distances to early-type galaxies (e.g., Tonry & Schneider 1988), but in our case the clusters are all at the same distance and the surface brightness fluctuations are caused by differences in age. One must exercise caution when using this technique for other galaxies, since the relationships derived below for M83 would need to be renormalized for galaxies at different distances.

We first need to remove the overall radial gradient in the cluster luminosity profile, since this gradient typically dominates over the peak-to-peak variations in pixel flux within the cluster. We accomplish this by creating a median divided image (with a 3×3 smoothing box size), which effectively flattens the radial profile of the cluster, leaving behind primarily the smaller scale pixel-to-pixel variations that we are interested in here. We then measure the RMS scatter in the fluxes of pixels located within a 10 pixel radius. A more sophisticated method is being developed by C. Kaleida et al. (2011, in preparation) where the RMS variations are measured within the half-light or effective radius $R_{\rm eff}$ of the cluster, hence accounting for clusters of different sizes in a more systematic manner.

Figure 5 shows a comparison of the F555W image and the median divided F555W image in a region including clusters younger than $\log(\tau/{\rm yr}) \approx 7.0$ (blue circles and labels) and older than this (red circles and labels). The RMS measurements are indicated in the bottom panel. One can easily see that old clusters (e.g., nos. 65 and 70) nearly disappear from the median divided image, resulting in low values of the RMS, while bright, individual stars are observed in the younger clusters (e.g., nos. 32 and 49), resulting in a higher RMS. Small, barely visible dust lanes also contribute to larger values of RMS for the young clusters. In a few very concentrated clusters there are small artifacts at their centers, for example in cluster no. 64. However, the RMS is dominated by pixels outside of this central region, hence this is a relatively small effect. We note that for four clusters, identified in Table 1, we have used a slightly smaller radius to avoid single bright stars that are almost certainly unrelated to the cluster (e.g., nos. 66, 69, 70 and 79).

In the upper panel of Figure 6 we plot the RMS in the pixel-to-pixel flux measured in the V band versus the morphological category. The resolution is better here for clusters younger than $\approx 10^7$ yr (i.e., category 3 and 4 objects). In the lower panel of Figure 6 we plot the RMS vs. the SED age, which gives better resolution for clusters older than $\approx 10^7$ yr. These figures

show the second main result of our work, *that older clusters have smaller RMS values of the pixel-to-pixel flux variations.* However, we also note, especially in the top panel, that the RMS is degenerate, and increases in strength over the age range 2–7 Myr (i.e., morphological categories 3 and 4), peaks in category 4, corresponding to an age of approximately 5–10 Myr, and decreases in strength for clusters with older ages and in later categories.

There are several possible explanations for this behavior. The first, and probably most important effect, is that the brightest stars (i.e., red and blue super giants) do not appear until about 5 Myr, and are largely gone by about 20 Myr. Two other evolutionary effects may potentially contribute to the low RMS measured for the very young clusters. (1) The central part of the cluster, where it is difficult to detect individual stars due to the high background, might emerge from its dust cocoon before the outskirts. (2) Clusters may start out very compact and expand with age. Hence crowding may make it impossible to detect individual stars at very early ages. There is both theoretical and observational support for both of these conjectures, as discussed below.

These trends are illustrated by the lines in Figure 6, which represent linear fits to observations. The best fits for the top panel are given by: $MC = (8.57 \pm 1.61) \times RMS + 2.85 \pm 0.18$ (i.e., a 5 σ correlation) for category <4.7, and $MC = (-7.23 \pm 1.25) \times RMS + 5.79 \pm 0.11$ (i.e., a 6 σ correlation) for category ≥ 4.7.

For the bottom panel, only the trend for older clusters is shown, with $\log(\tau/\mathrm{yr}) = (20.43 \pm 5.43) \times RMS + 9.59 \pm 0.31$ for $\log(\tau/\mathrm{yr}) > 7$. We will better quantify the correlation between cluster age and the RMS in pixel-to-pixel fluxes in a future paper using a significantly larger number of clusters. We note that these relationships will be different for galaxies at different distances, and in different filters. For example, fluctuations will generally be larger for older clusters (100–1000 Myr) in the near-IR due to the presence of asymptotic giant branch (AGB) stars.

Values of RMS pixel-to-pixel flux variations for each cluster are included in Table 1, and the mean values for clusters in each morphological category are included in Table 2. The RMS method is particularly promising for estimating the ages of clusters between 10 and 100 Myr, a range which can be somewhat difficult for the SED method because the integrated colors of clusters loop back on themselves during this period. Clusters in this age range can be identified initially by their lack of ionized gas.

It is instructive to look at the outliers in Figure 6, just as we did for the correlation between SED age and morphological category in Section 3.1. In the bottom panel the cluster with RMS = 0.03 and $\log(\tau/\mathrm{yr}) = 6.8$ (ID = 44034) is an apparent outlier. It is also one of the sources which we believe, based on the discussion in Section 3.1, has an incorrect SED

age estimate. Based on its measured colors and assuming $E(B-V) = 0.0$ instead of 0.28, this cluster has a likely age of $\log(\tau/\mathrm{yr}) \approx 7.8$, more appropriate for it's low RMS value. Similarly, many of the data points just to the right of this one are the same category 5b outliers discussed in Section 3.1 that have suspect ages. Other data points in the same region of the $\log(\tau/\mathrm{yr})$ versus RMS plot are located in the large bubble just below the nucleus of M83, where it is difficult to measure the RMS accurately due to the very high background. We note that the four clusters with RMS < 0.07 and $\log(\tau/\mathrm{yr}) < 6.5$ are all in morphological category 3, and are largely responsible for the decline in the measured RMS for the youngest clusters.

Many of the trends discussed above are seen in Table 2, which lists the mean values of several parameters as a function of morphological category. In particular, the trends in $E(B-V)$, $\log(\tau/\mathrm{yr})$, and Hα shell radius (when present) are clearly evident. In addition, the double-valued nature of pixel-to-pixel RMS values is evident, with a peak at category 4a. One correlation that was mentioned briefly is the trend of increasing cluster size with age, quantified by the increase in the concentration index (CI) from values around 2.5 for Categories 3 and 4a to > 3.0 for Categories 5b and 6. We find the same trend in our M51 data, which is briefly discussed in the Appendix. This effect appears to be real, and is likely related to the rapid expansion of the clusters (see, for example, Mackey & Gilmore 2003; Bastian et al. 2009; Pfalzner 2009). Several different physical mechanisms may be responsible for this expansion, including the expulsion of leftover ISM due to feedback from massive stars (e.g., Goodwin & Bastian 2006; Baumgardt & Kroupa 2007), and heating by binary stars and stellar mass black holes (e.g., Mackey et al. 2008; see Portegies Zwart et al. 2010 for a review of this subject). The early expansion of star clusters will be discussed in more detail in a future paper (R. Chandar et al. 2011, in preparation).

5. "Single Star" HII Regions

While the dominant sources of ionizing flux responsible for the Hα emission in M83 are massive, young star clusters, which were studied in the previous sections, there is also a population of compact HII regions which are ionized by what appear to be single stars. In this section we identify and study a sample of 22 HII regions with very small Hα radii and an unresolved central point source (based on their CI, i.e., the magnitude difference between 0.5 and 3 pixel radii; see Chandar et al. 2010). Color images of the selected sources are shown in Figure 7. Only the brighter candidates have been retained for this first exploratory study; the sample could be increased by a factor of two or more if fainter, less distinct objects were included. The measured colors of these sources, shown in Figure 8, either coincide with the

colors predicted for the bluest (youngest) stars in the upper left portion of the diagram, or are found downstream along the reddening vector. Basic properties of these sources, including positions, M_V, CI, colors and measured radii of the Hα bubble, are compiled in Table 3.

We note that it is unlikely that all of these objects are actually individual massive stars, hence the use of quotes around "Single Star." Some, or even most of these may be a dominant star among a close grouping of stars which are either too close to the primary source, or too faint, to be detected. What we can say is that a single (or very close binary) star dominates the light profile, resulting in a CI that is indistinguishable from a single star.

If we assume that all of these objects have a similar age, and that the distribution in the two-color diagram is primarily due to reddening, we can correct for the effects of reddening and extinction. We show the corrected photometry in a color magnitude diagram in the left panel of Figure 8. Here, we have assumed an intrinsic color of $U-I = -2.2$, the color of the bluest object, and solve for the $V-I$ color excess of each HII region. We find that this procedure moves most of the objects to a very young isochrone (4 Myr is shown), although three sources scatter to the left of the models. These may be especially young stars, or the offset may result from observational uncertainties, since these are the three most reddened sources, and hence have the largest corrections.

While many of these single-star HII (i.e., SSHII) regions are found near large regions of recent star formation, several of them are quite isolated (see Figure 3 from Whitmore 2010), raising the possibility that these massive stars formed in the field rather than in clusters or associations. For example, five of the 22 SSHII regions are ≈1 kpc away from any region of active star formation. If these are stars that have been dynamically ejected from their birthsites, i.e., runaways, they must have velocities ≈200 km/s. However, they do not appear to have the prominent bow-front morphologies typical of many runaway stars in the Galaxy and Magellanic Clouds (e.g., Gvaramadze et al. 2011). Velocity measurements are needed to establish if these massive stars formed in the field or are runaways from larger star-forming regions.

6. Discussion

As summarized in the Introduction, the spatial relationship between young $\tau \lesssim 10^7$ yr star clusters and their HII regions has been previously studied both observationally and theoretically. To our knowledge however, no study has yet systematically measured the sizes of Hα bubbles in a nearby galaxy and correlated these sizes with the properties of their ionizing star clusters, as we have done here. We have demonstrated that in M83 there is a

good correlation between bubble size and age for clusters younger than $\log(\tau/\mathrm{yr}) \approx 6.7$, and that clusters with ages $\log(\tau/\mathrm{yr}) \approx 6.7$–6.9 have a larger range in bubble size. This suggests that some of the expanding bubbles at these older ages may have effectively "stalled."

Theoretical work suggests that bubble size should depend not only on the ambient pressure in the ISM and the age of the cluster, but also on cluster mass. To look for evidence of a mass-dependence on bubble size, we compare the sizes measured for Hα bubbles associated with $\log(\tau/\mathrm{yr}) = 6.7$–6.9 clusters that are more and less massive than 10^4 $M_\odot$. At these ages the bubbles are presumably approaching their stall radius, and the effect of cluster mass should be more apparent. The large, open circles in the top panel of Figure 4 show the sizes of clusters with $M < 1 \times 10^4$ $M_\odot$ and $\log(\tau/\mathrm{yr}) > 6.7$. While clusters at high and low masses have an overlapping range in cluster size, there is a tendency for more massive clusters to have larger bubbles, with median sizes of 18 pc and 41 pc for $M < 10^4$ $M_\odot$ and $M \geq 10^4$ $M_\odot$, respectively. A formal fit of Hα radius versus $\log(M/M_\odot)$ for these clusters gives a slope of 0.006 ± 0.005, suggesting that there may be a weak correlation between bubble size and mass. Future studies that include a larger number of sources, selected in a more systematic way, are needed to confirm this result.

However, other effects may also be important. For example, stochasticity in the number of massive stars formed in lower mass clusters can strongly affect their integrtated colors and hence their estimated ages. In this case, a lower mass cluster can have an intrinsically redder color than a higher mass cluster of the same age (e.g., Fouesneau & Lancon 2010), and hence an older estimate for the age of the cluster.

In addition to the correlation between Hα bubble size and cluster age (and possibly mass), we also found that the RMS variations in pixel-to-pixel brightness correlates with cluster age. This result has applications beyond star clusters, and can be used to constrain the ages of stellar populations in general. For example, portions of M83 itself that contain young stars and star clusters, such as along the spiral arms, have larger pixel-to-pixel flux variations than portions of M83 dominated by older stars, such as between the arms (see H. Kim et al. 2011, in preparation for a discussion). This is also true in large portions of M82 and in portions of the tidal tails of galaxy mergers, where regions dominated by intermediate age star clusters (≈100 Myr) have small fluctuations in the surface brightness of the field stars.

7. Summary and Conclusions

We have used observations taken with the newly installed WFC3 camera on-board the *Hubble Space Telescope* to develop two independent methods for age-dating young star clusters in the nearby spiral galaxy M83. Our primary results are summarized below.

1. A working classification system, largely based on Hα morphology and pixel-to-pixel flux variations, was developed to map an observed age sequence onto a proposed sequence of cluster evolution. The underlying evolutionary picture includes the formation of dense cores in giant molecular clouds (GMCs); a stage where the young stars are completely obscured by their dust cocoon; an emerging stage where the clusters become visible in the IR, and then in the optical as stellar winds and supernovae blow away the dust; a stage where an expanding Hα bubble is blown and the existence of very bright young stars leads to large pixel-to-pixel flux variations; and later stages with no evidence of Hα and diminishing pixel-to-pixel flux variations.

2. We found that Hα morphology, i.e., the size of the ionized gas bubble, provides a viable method for age-dating clusters in the range 1–10 Myr. This method is based on the simple premise that the gas in very young ($\tau <$ few Myr) clusters is largely coincident with the cluster stars, is in a small, ring-like structure surrounding the stars in slightly older clusters since the winds from massive stars have had time to push out the natal gas (e.g., $\tau \approx 5$ Myr), and is in a larger ring-like bubble for still older clusters (i.e., $\approx$5–10 Myr). If no Hα is associated with a cluster it is generally older than $\approx$10 Myr.

We first made *qualitative* estimates based on the classification scheme outlined above, and find that the ages of the clusters, as determined from the SED method described in Chandar et al. (2010), correlate well with the morphological categories, with a scatter of $\approx$0.1 in $\log(\tau/\mathrm{yr})$ within each category for the clusters with Hα emission, and a scatter of $\approx$0.5 in $\log(\tau/\mathrm{yr})$ for the older clusters. We then *quantified* this technique by correlating the measured radii of the most conspicuous Hα-emitting ring or shell which appears to be physically related to the cluster with the SED ages determined in Chandar et al. (2010). We found tentative evidence for a weak correlation between bubble size and cluster mass, but a larger, more objectively selected sample will be required to confirm this.

3. We then used pixel-to-pixel flux variations to age-date clusters. This technique is based on the fact that individual stars are bright enough to be visible within clusters when they are young (e.g., $M_V < -3.5$, the approximate detection level, for the brightest stars with ages <100 Myr), leading to relatively large pixel-to-pixel variations in flux. The strength of the fluctuations peaks in clusters with ages of $\approx$5–10 Myr, presumably because this is when the brightest stars (e.g., red and blue super giants) appear. The number of luminous,

evolved stars falls off for both younger and older clusters. This degeneracy in age can be broken using other age indicators such as the Hα morphology. The technique is especially useful for identifying clusters older than 100 Myr.

4. A by-product of this study was the identification of 22 "single-star" HII regions in M83. By assuming that all of these objects have a similar age, and that the distribution in the two-color diagram is primarily due to reddening, we corrected for the effects of reddening and extinction. We found that this procedure moves most of the objects to a very young isochrone with an age approximately 4 Myr. Some of these massive stars are located far from any star-forming region, indicating that they either formed in the field or were dynamically ejected from their birthsites at very high velocities. These SSHII regioins will be studied in more detail in H. Kim et al. (2011, in preparation).

In the future, we will extend the classification system into the near-IR (i.e., categories 1 and 2) using our J and H observations. We will also calculate the energy budget of cluster stars and compare with physical properties of the clusters and the ISM. Finally, we will extend this analysis to other galaxies in the ERS1 sample (including "low pressure" systems such as the dwarf starburst galaxy NGC 4214) in order to determine whether the relationships are universal or are strongly dependent on environment.

We thank Zolt Levay for making the color images used in Figures 1 and 2. This paper is based on observations taken with the NASA/ESA *Hubble Space Telescope* obtained at the Space Telescope Science Institute, which is operated by AURA, Inc., under NASA contract NAS5-26555. The paper makes use of Early Release Science observations made by the WFC3 Science Oversight Committee. We are grateful to the Director of STScI for awarding Director's Discretionary time for this program. R. C. is grateful for support from the NSF through CAREER award 0847467. This research has made use of the NASA/IPAC Extragalactic Database (NED), which is operated by the Jet Propulsion Laboratory, California Institute of Technology, under contract with NASA.

Facilities: HST.

Appendix

The spiral galaxy M51 was originally used to perform a pilot study to test how well Hα morphology can be used to estimate cluster ages. Examples of the results are included in Figures 9 and 10. These are similar to Figure 2 for M83 and show that even at twice the distance of M83 the quality of the images are comparable, and the morphological categories match SED age estimates at a similar level. A more complete analysis will be included in a future paper (R. Chandar et al. 2011; in preparation).

REFERENCES

Andre, P., Ward-Thompson, D., & Barsony, M. 1993, ApJ, 406, 122

Bastian, N., Trancho, G., Konstantopoulos, I. S., & Miller, B. W. 2009, ApJ, 701, 607

Baumgardt, H., & Kroupa, P. 2007, MNRAS, 380, 1589

Bica, E., & Alloin, D. 1986, A&AS, 666, 171

Bruzual, G., & Charlot, S. 2003, MNRAS, 344, 1000

Chandar, R., Whitmore, B. C., & Fall, S. M. 2010, ApJ, 719, 966

Dopita, M. A., et al. 2006a, ApJ, 647, 244

Dopita, M. A., et al. 2006b, ApJS, 167, 177

Dopita, M., et al. 2010, ApJ, 710, 964

Fouesneau, M., & Lancon, A. 2010, A&A, 521, 22

Gao, Y., & Solomon, P. 2004, ApJ, 606, 271

Goodwin, S. P., & Bastian, N. 2006, MNRAS, 373, 752

Gvaramadze, V. V., Kroupa, P., Pflamm-Altenburg, J. 2011, A&A, 525, A17

Israel, F. P. 1978, A&A, 70, 769

Lada, C. J., & Lada, E. A. 2003, ARA&A, 41, 57

Mackey, A. D., & Gilmore, G. F. 2003, MNRAS, 338, 85

Mackey, A. D., Wilkison, M. I., Davies, M. B., & Gilmore, G. F. 2008, MNRAS, 386, 65

Oey, M. S., & Clarke, C. J. 1997, MNRAS, 289, 570

Oey, M. S., & Clarke, C. J. 1998, AJ, 115, 1543

Oey, M. S., & Garcia-Segura, G. 2004, ApJ, 613, 302

Oey, M. S., & Massey, P. 1995, ApJ, 452, 210

Pfalzner, S. 2009, A&A, 498, L37

Portegies Zwart, S. F., McMillan, S. L. W., & Gieles, M. 2010, ARA&A, 48, 431

Schweizer, F., & Seitzer, P. 1993, ApJ, 417, L29

Searle, L., Wilkinson, A., & Bagnuolo, W. G. 1980, ApJ, 239, 803

Thim, F., Tammann, G. A., Saha, A., Dolphin, A., Sandage, A., Tolstoy, E., & Labhardt, L. 2003, ApJ, 590, 256

Tonry, J., & Schneider, D. P. 1988, AJ, 96, 807

Walborn, N. R. 2002, in ASP Conf. Ser. 267, Hot Star Workshop III: The Earliest Phases of Massive Star Birth, ed. P. A. Crowther (San Francisco, CA: ASP), 111

Walborn, N. R. 2010, in ASP Conf. Ser. 425, Hot And Cool: Bridging Gaps in Massive Star Evolution, ed. C. Leitherer, Ph.D. Bennett, P.W. Morris, & J.Th. van Loon (San Francisco, CA: ASP), 45

Walborn, N. R., & J. Wm. Parker, ApJL, 399, L87, 1992

Weaver, R., McCray, R., Castor, J., Shapiro, P., & Moore, R. 1977, ApJ, 218, 377

Whitmore, B. C. 2010 in ASP Conf. Ser., UP: Have Observations Revealed a Variable Upper End of the Initial Mass Function, ed. M. Treyer et al. (San Francisco, CA: ASP), 141, in press

Whitmore, B. C., Zhang, Q., Leitherer, C., Fall, S. M., Schweizer, F., & Miller, B. W. 1999, AJ, 118, 1551

Whitmore, B. C., et al. 2010, AJ, 140, 75

Wilking, B. A., Lada, C. J., & Young, E. T. 1989, ApJ, 340, 823

Wofford, A., Leitherer, C., & Chandar, R. 2010, ApJ, 727, 100

This preprint was prepared with the AAS LaTeX macros v5.2.

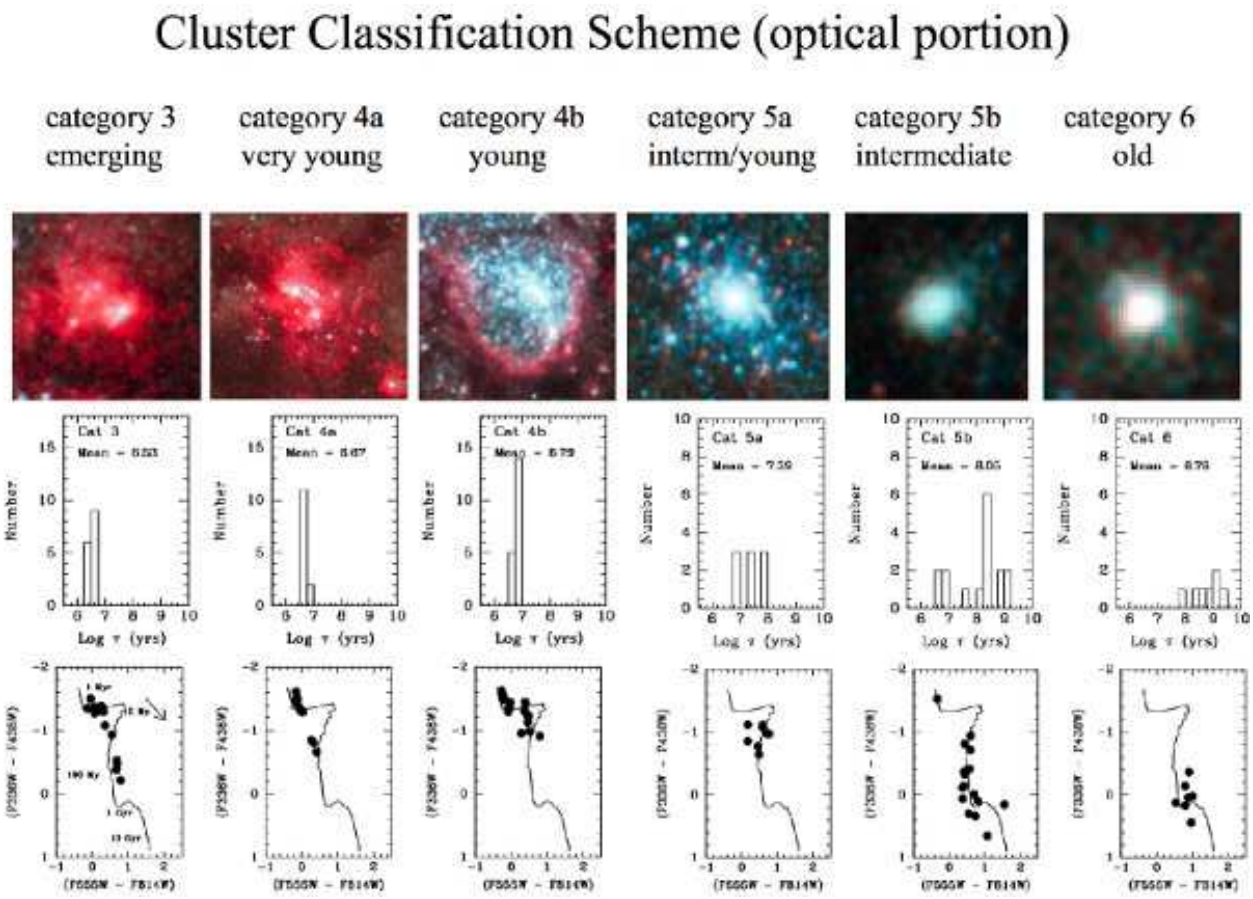


Fig. 1.— Examples of sources in the various categories defined in Section 2 are shown along the top row; histograms of the SED age estimates for the clusters in Table 1 (from Chandar et al. 2010) are in the middle row, and two-color diagrams comparing the (measured) integrated colors of the clusters with predictions for a twice solar metallicity BC09 model (G. Bruzual & S. Charlot 2009, private communication; see also Bruzual & Charlot 2003) are shown along the bottom row.

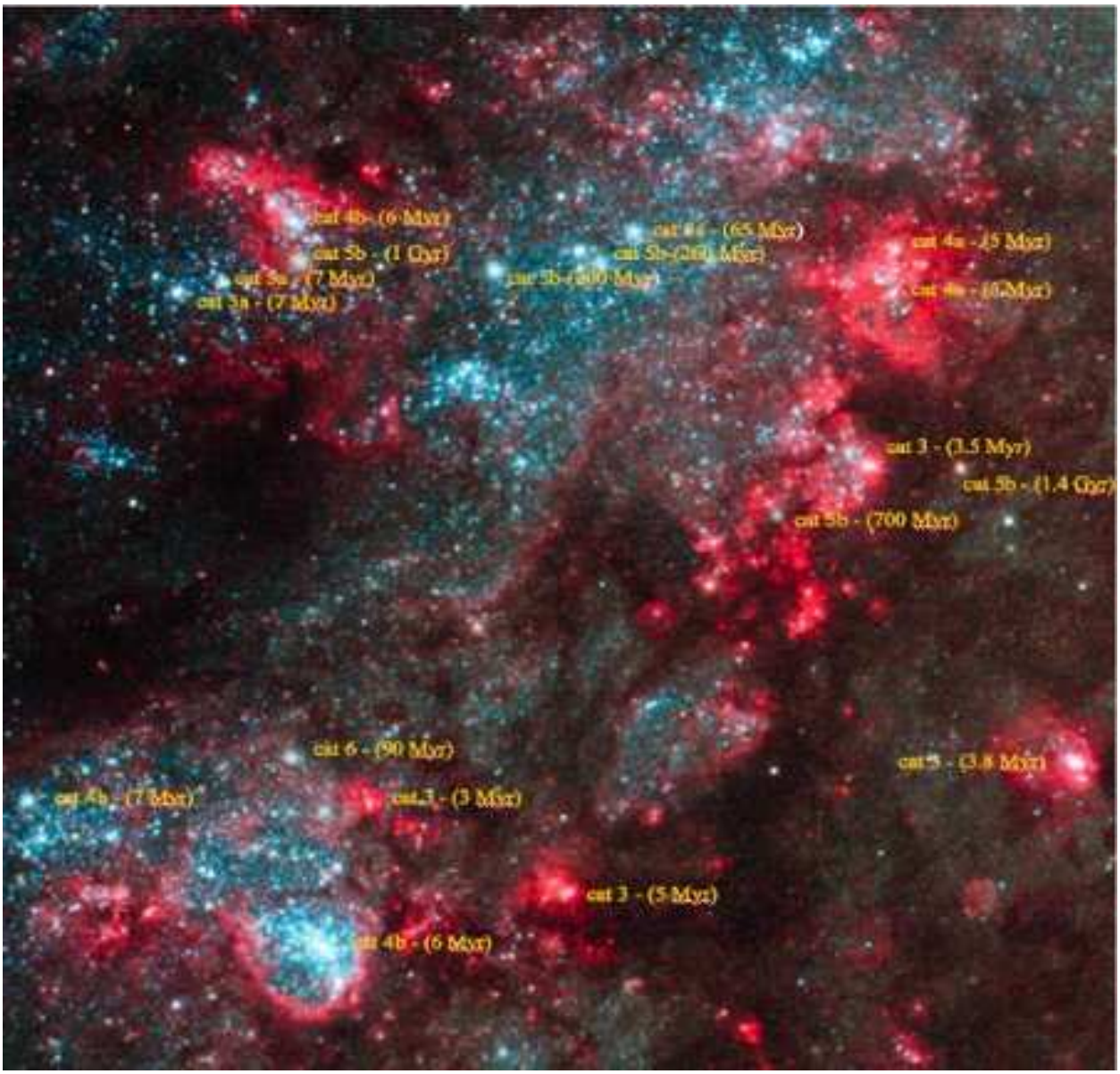


Fig. 2.— Portion of the M83 field (1.0 × 1.0 kpc) showing the good correlation between morphological categories determined in this paper and SED age estimates from Chandar et al. (2010).

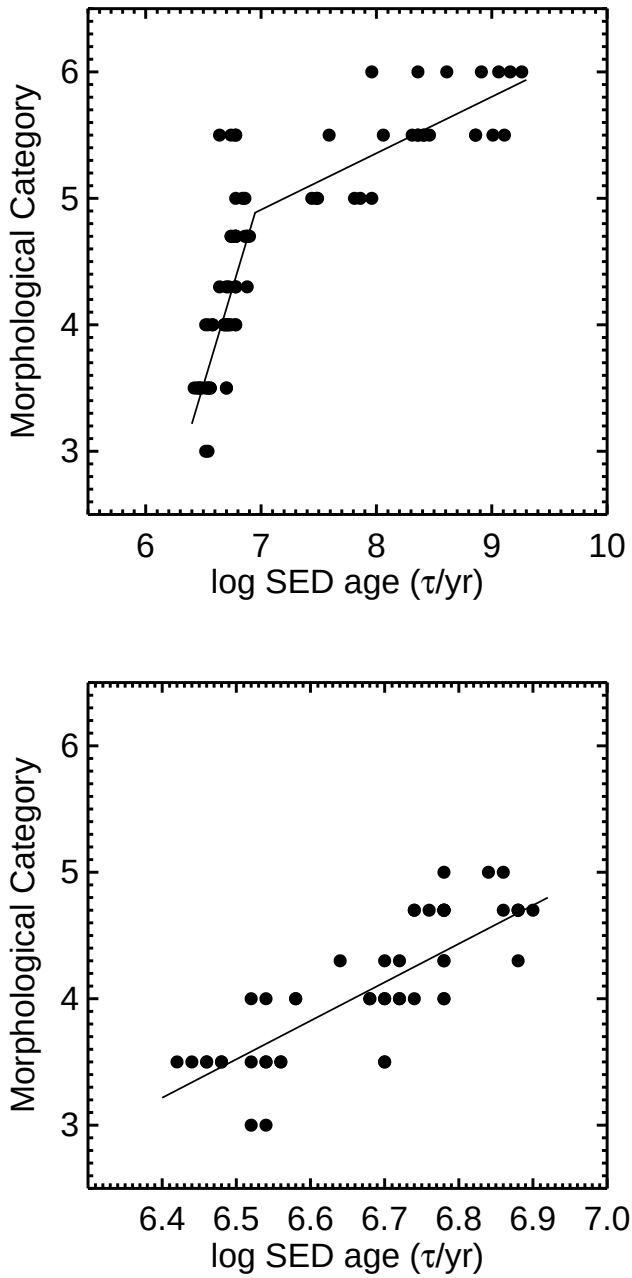


Fig. 3.— Plot of morphological categories versus log SED age estimates. Note how the scatter increases with age and that the relationship is nonlinear, as expected since Hα morphology evolves quickly between the ages of a few to 10 Myr. The bottom panel shows an enlargement for the younger ages. The best linear fit is shown in both panels.

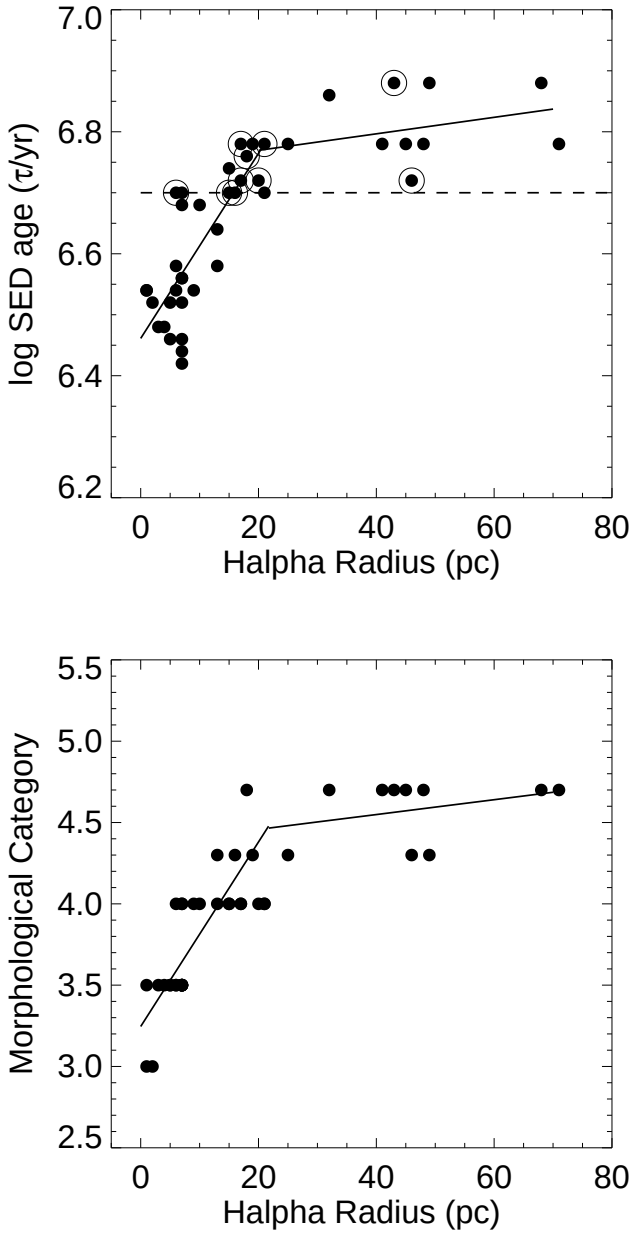


Fig. 4.— Plot of the Hα bubble radius vs log SED ages in the upper panel and morphological category in the lower panel. The correlation is similar to the relationship shown in Figure 3, but with fewer outliers and hence smaller scatter. The large, open circles in the top panel show the sizes of clusters with $M < 1 \times 10^4\ M_\odot$ and $\log(\tau/\mathrm{yr}) \geq 6.7$, as discussed further in Section 6.

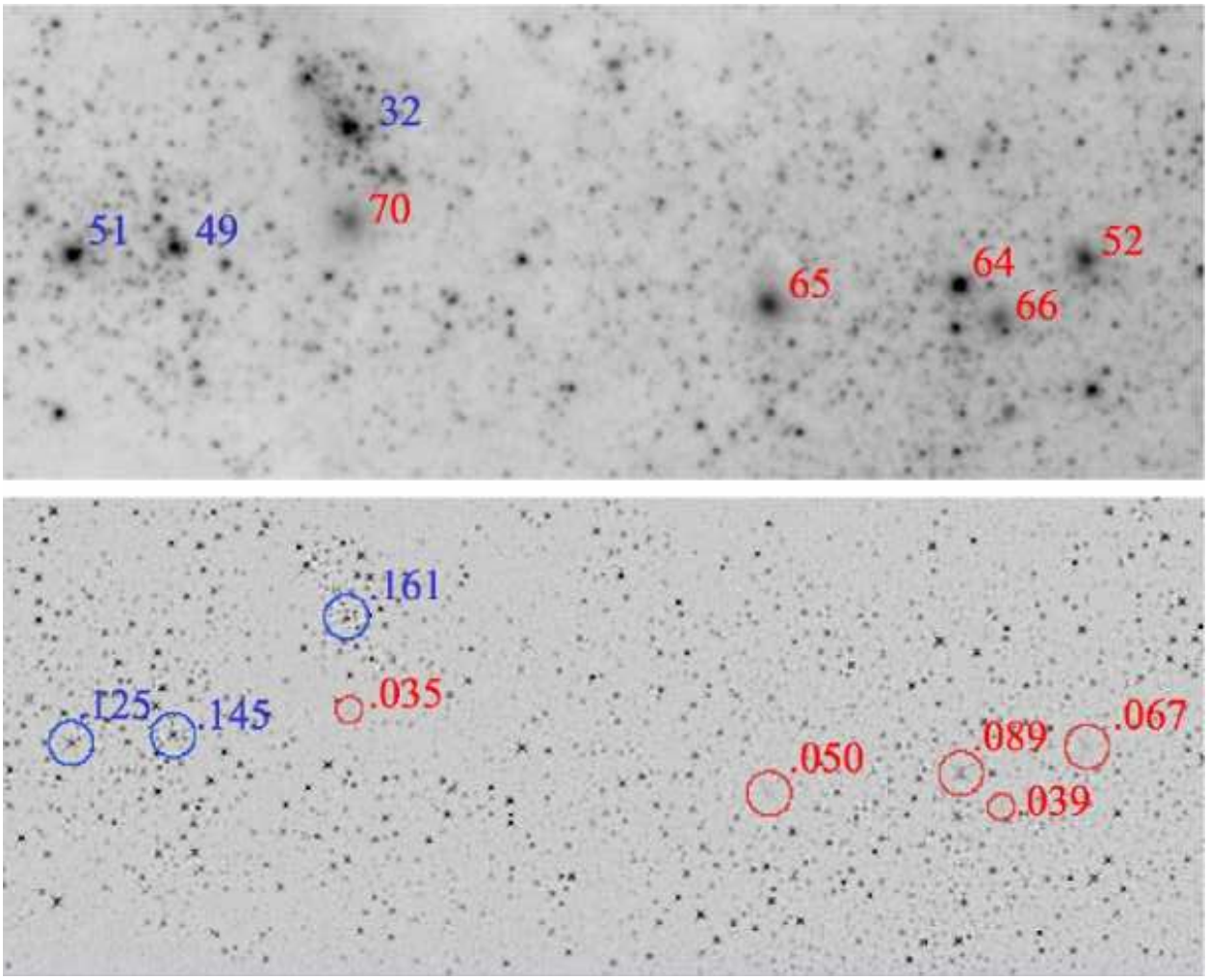


Fig. 5.— Top: F555W image (log stretch) for a portion of M83 (i.e., the upper left of Figure 2). Blue labels are used for clusters younger than 10 Myr while red labels are used for clusters older than 10 Myr. Bottom: median divided image for the same region with the aperture size and rms of the pixel-to-pixel flux variations shown.

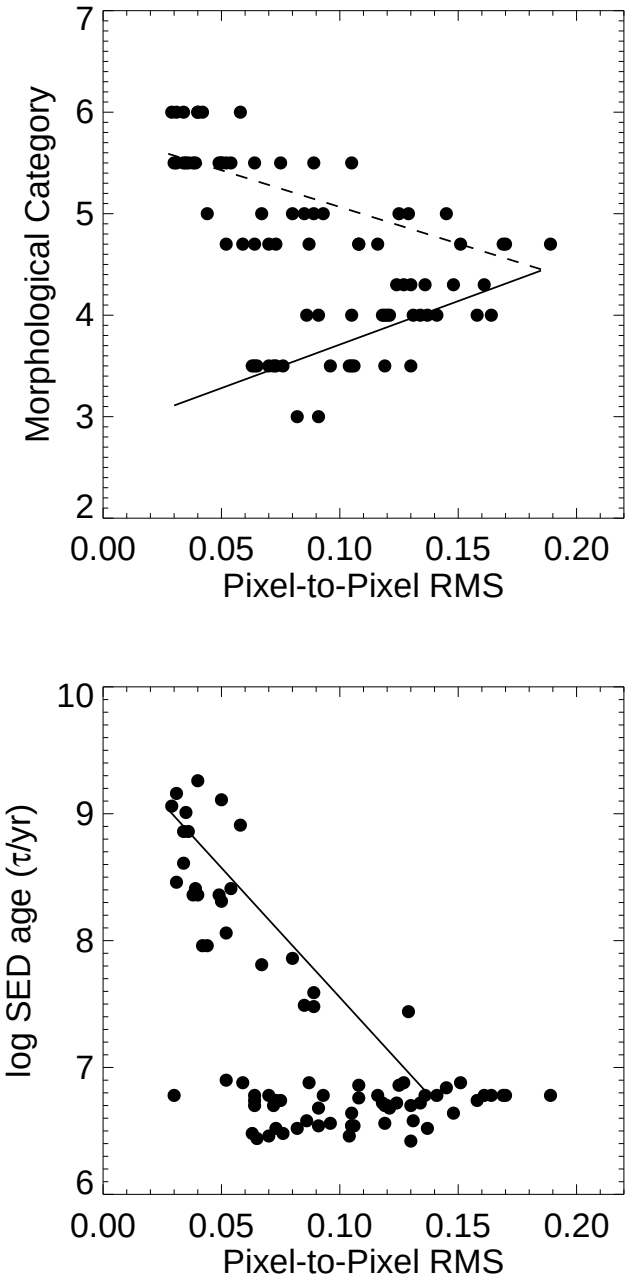


Fig. 6.— Plot of the pixel-to-pixel flux variation (RMS) versus log SED age in the lower panel, and morphological category in the upper panel. The highest values of the RMS are seen in the 5–10 Myr range (category 4b), with lower values for both younger and older clusters. Note that nearly all the clusters with RMS < 0.05 have ages greater than 100 Myr.

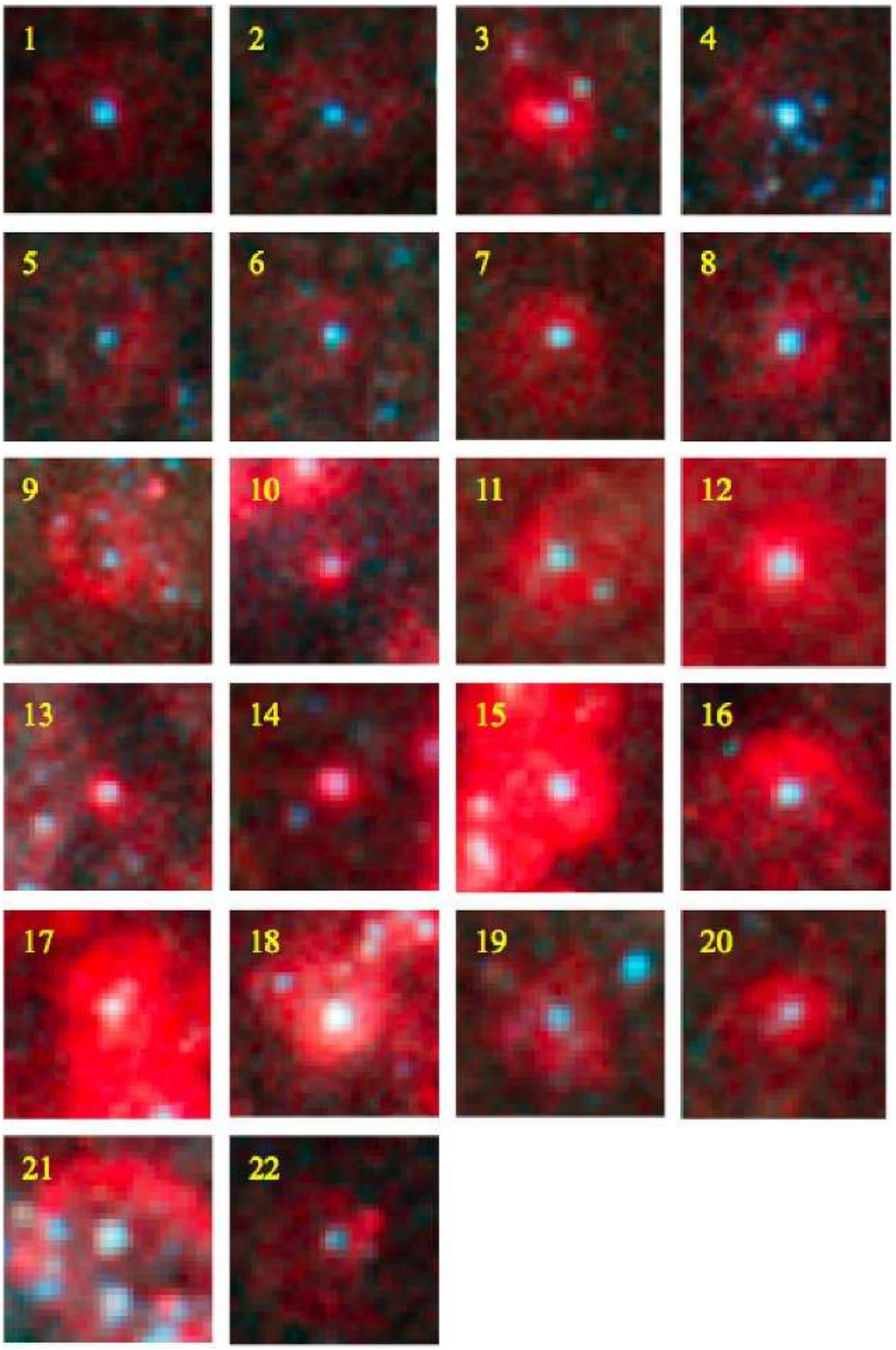


Fig. 7.— Mosaic of the 22 SSHII region candidates.

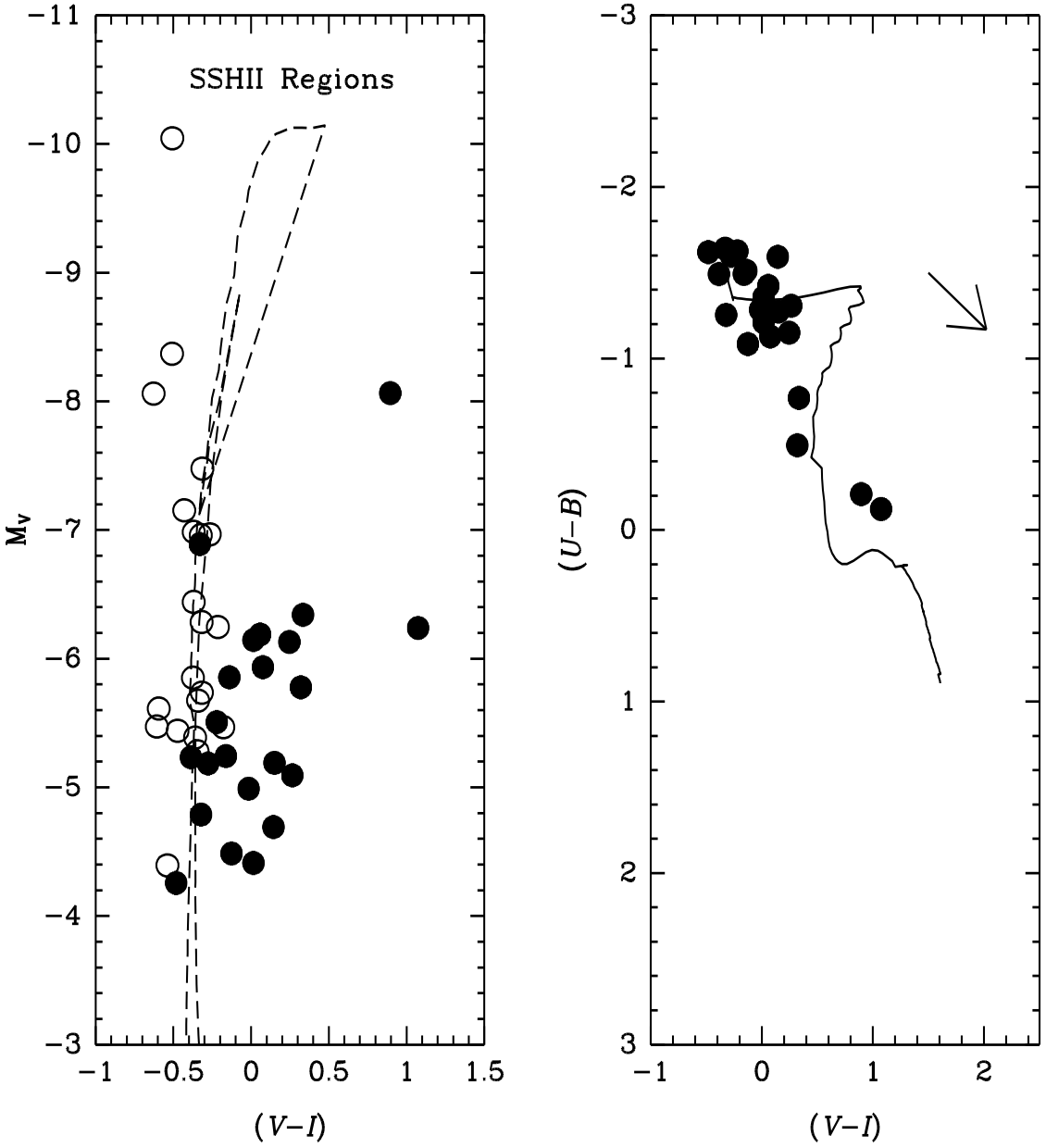


Fig. 8.— Left: Color-magnitude diagram for the SSHII region sample. The filled circles show the observed values while the open circles show the corrected values based on the extinction derived from the color-color diagram (see the text). Right: Color-color diagram for the SSHII region sample.

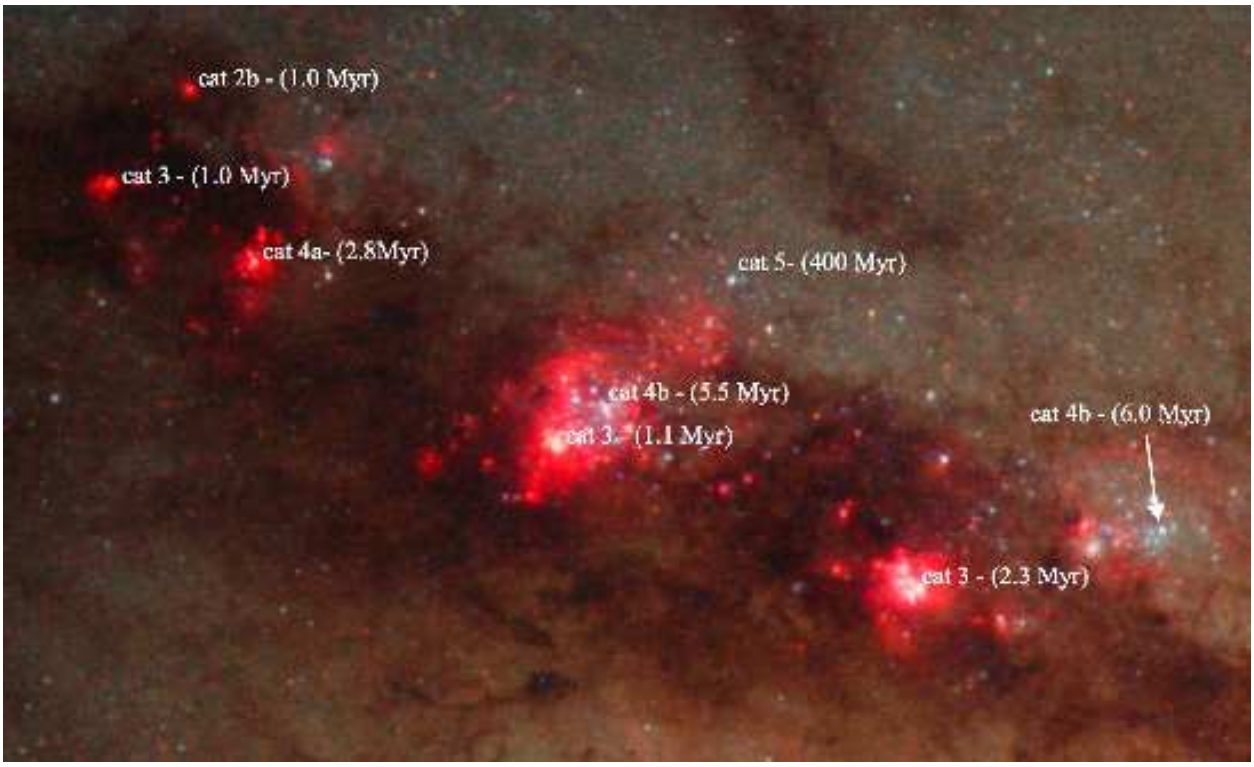


Fig. 9.— Portion of the M51 image showing the good correlation between morphological categories and SED age estimates (R. Chandar et al. 2011, in preparation). Note the similarity with Figure 2, implying that this method of age dating will work to at least twice the distance of M83.

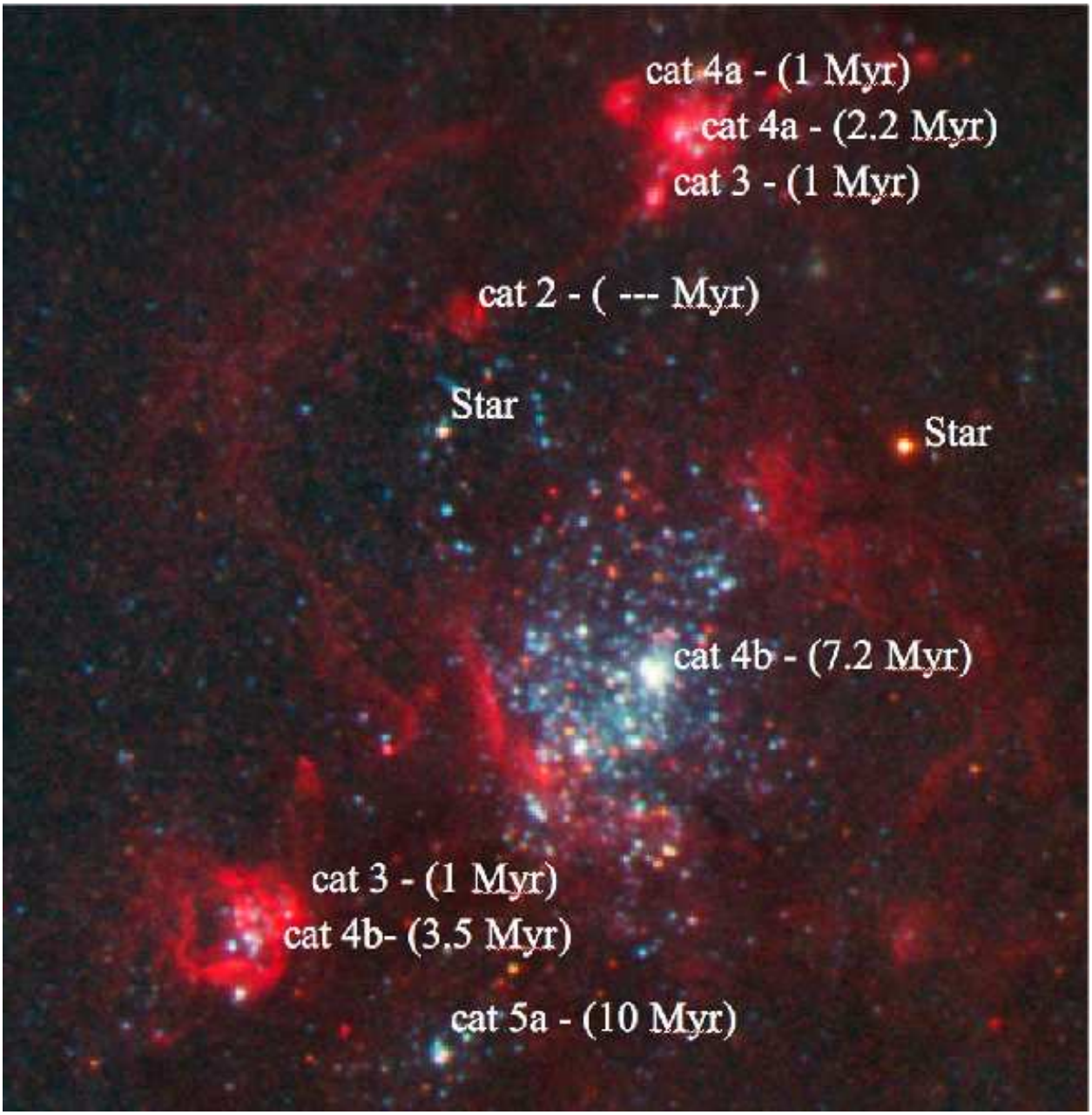


Fig. 10.— Similar to Figure 9, but for a different region.

Table 1. Parameters for 88 Selected Clusters

#	ID	RA	DEC	M_V[a] (mag)	CI[b] (mag)	$U-B$[a] (mag)	$V-I$[a] (mag)	$E(B-V)$ (mag)	Log Age (yr)	Mass ($M_\odot$)	Cat[c]	R(Hα) (pc)	RMS[d]
1	65815	204.244637	−29.8507043	−6.10	2.57	−1.35	−0.12	0.24	6.52	1.1E3	3	2	0.082
2	63611	204.2426354	−29.8515924	−6.42	2.35	−1.27	0.07	0.34	6.54	2.1E3	3	1	0.091
3	41736	204.251687	−29.8640556	−8.70	2.68	−0.21	0.80	0.50	6.7	2.6E4	3	7	0.064
4	39744	204.2524132	−29.8651911	−11.03	2.58	−1.33	0.23	0.30	6.56	1.2E5	3	7	0.119
5	49651	204.2564416	−29.8586912	−7.17	2.50	−0.38	0.68	0.50	6.48	7.1E3	3	3	0.063
6	32461	204.2880034	−29.8692326	−7.67	2.62	−1.36	0.30	0.44	6.52	8.6E3	3	5	0.073
7	53072	204.2889299	−29.8569125	−6.64	2.61	−0.93	0.56	0.50	6.48	4.2E3	3	4	0.076
8	93801	204.2795357	−29.8392001	−7.10	2.50	−1.37	0.08	0.32	6.54	3.6E3	3	1	0.106
9	50287	204.2865616	−29.8582915	−7.35	2.66	−0.54	0.69	0.50	6.70	7.4E3	3	6	0.072
10	59214	204.2818977	−29.8537395	−7.56	2.53	−1.08	0.36	0.50	6.54	9.3E3	3	6	0.105
11	24767	204.2493318	−29.8729735	−6.89	2.32	−0.46	0.70	0.50	6.56	5.1E3	3	7	0.096
12	58013	204.2475174	−29.8543366	−6.49	2.43	−1.29	0.15	0.42	6.46	5.4E3	3	7	0.104
13	52726	204.2458956	−29.8570619	−8.13	2.78	−1.50	−0.06	0.26	6.42	1.2E4	3	7	0.130
14	12721	204.2908632	−29.8785688	−5.98	2.43	−1.30	0.32	0.50	6.46	4.3E3	3	5	0.070
15	19354	204.2525635	−29.8755537	−6.06	2.83	−1.39	0.27	0.44	6.44	2.5E3	3	7	0.065
16	51616	204.2799185	−29.8575701	−9.31	2.43	−1.33	−0.02	0.20	6.58	1.8E4	4a	6	0.131
17	49790	204.2546965	−29.8585957	−7.88	2.27	−0.85	0.27	0.42	6.68	1.1E4	4a	10	0.091
18	17035	204.2906967	−29.8766101	−7.23	2.24	−1.48	−0.16	0.00	6.70	1.8E3	4a	15	0.119
19	66897	204.2654298	−29.8502774	−8.60	2.96	−1.50	−0.12	0.00	6.72	4.4E3	4a	20	0.134
20	39842	204.2520397	−29.8651314	−10.94	2.71	−1.51	−0.15	0.08	6.58	5.2E4	4a	13	0.086
21	31457	204.2855284	−29.8698283	−8.83	2.19	−1.31	−0.03	0.04	6.78	8.9E3	4a	17	0.164
22	74860	204.262148	−29.8474511	−8.59	2.67	−1.43	−0.14	0.00	6.78	5.5E3	4a	21	0.141
23	89929	204.2581863	−29.8412261	−6.79	2.23	−1.35	−0.05	0.04	6.72	1.3E3	4a	17	0.118
24	25607	204.2492229	−29.8725982	−7.85	2.61	−0.66	0.42	0.50	6.70	1.2E4	4a	21	0.120
25	75041	204.2775285	−29.847385	−7.31	2.24	−1.61	−0.15	0.12	6.52	2.7E3	4a	7	0.137
26	64462	204.2811447	−29.8512236	−8.19	2.30	−0.81	0.34	0.46	6.68	1.7E4	4a	7	0.121
27	61923	204.263904	−29.8523354	−6.02	2.52	−1.28	0.06	0.36	6.54	1.5E3	4a	9	0.105
28	21601	204.2861725	−29.8744932	−9.59	2.27	−1.48	−0.12	0.00	6.74	1.5E4	4a	15	0.158
29	62771	204.2811659	−29.8519608	−7.25	2.27	−0.96	0.28	0.38	6.70	5.6E3	4a	16	0.130
30	13265	204.2547344	−29.8783208	−7.64	2.44	−1.63	−0.27	0.00	6.64	2.3E3	4a	13	0.148
31	5990	204.2551409	−29.8813282	−8.17	2.47	−1.53	−0.26	0.00	6.72	3.9E3	4a	46	0.124
32	67958	204.2887307	−29.8499286	−9.84	3.20	−1.35	−0.04	0.02	6.78	1.1E4	4a	19	0.161
33	66054	204.2644967	−29.8506016	−9.97	2.63	−1.45	0.39	0.00	6.88	2.8E4	4a	49	0.127
34	69793	204.2694643	−29.8493238	−11.41	2.63	−1.48	−0.16	0.00	6.78	7.5E4	4a	25	0.136

Table 1—Continued

#	ID	RA	DEC	M_V[a] (mag)	CI[b] (mag)	$U-B$[a] (mag)	$V-I$[a] (mag)	$E(B-V)$ (mag)	Log Age (yr)	Mass (M⊙)	Cat[c]	R(Hα) (pc)	RMS[d]
35	7716	204.2816067	−29.8807039	−9.17	2.47	−1.43	0.41	0.00	6.88	1.4E4	4b	68	0.151
36	36651	204.2524088	−29.8668398	−12.17	3.09	−1.58	−0.22	0.00	6.78	1.1E5	4b	··· [e]	0.070
37	35937	204.2537197	−29.8672182	−10.31	2.79	−1.24	0.45	0.02	6.90	4.2E4	4b	··· [e]	0.052
38	54268	204.2932226	−29.8563319	−8.57	2.87	−0.91	0.79	0.34	6.86	1.7E4	4b	32	0.108
39	23366	204.2529648	−29.8736403	−9.39	2.43	−1.29	−0.08	0.02	6.78	1.3E4	4b	41	0.116
40	27423	204.2896066	−29.8718058	−8.38	2.34	−0.99	0.50	0.36	6.78	1.4E4	4b	71	0.170
41	78807	204.2629122	−29.8459862	−9.71	2.46	−1.55	−0.23	0.00	6.78	1.6E4	4b	45	0.169
42	36729	204.2525635	−29.8667944	−12.15	3.08	−1.45	0.00	0.00	6.74	1.0E5	4b	··· [e]	0.073
43	70777	204.2607456	−29.8489709	−8.18	2.68	−1.23	0.49	0.08	6.88	6.7E3	4b	43	0.087
44	70769	204.2650559	−29.8489734	−7.77	2.92	−1.34	−0.08	0.00	6.76	2.1E3	4b	18	0.108
45	37589	204.2519048	−29.8663287	−11.96	3.20	−1.13	0.46	0.24	6.74	1.4E5	4b	··· [e]	0.064
46	49893	204.2897929	−29.8585381	−9.76	2.74	−1.49	−0.24	0.00	6.78	1.6E4	4b	48	0.189
47	37095	204.2523893	−29.8665896	−11.18	2.79	−1.32	0.35	0.00	6.88	8.0E4	4b	··· [e]	0.059
48	78154	204.257905	−29.8462475	−8.28	2.76	−0.86	0.18	0.00	7.86	3.4E4	5a	···	0.080
49	66216	204.2897363	−29.8505371	−8.87	2.56	−0.98	0.70	0.34	6.84	2.5E4	5a	···	0.145
50	76156	204.2556622	−29.8469956	−10.21	3.15	−1.08	0.62	0.06	7.48	1.0E5	5a	···	0.089
51	66123	204.2903301	−29.8505755	−9.39	2.50	−1.11	0.59	0.22	6.86	3.0E4	5a	···	0.125
52	66069	204.2844254	−29.8505955	−8.88	3.13	−0.78	0.47	0.06	7.81	4.5E4	5a	···	0.067
53	85836	204.2694279	−29.8431197	−9.43	3.25	−1.12	0.18	0.10	6.78	8.7E3	5a	···	0.093
54	40779	204.2926898	−29.8645926	−10.17	3.06	−0.65	0.49	0.08	7.96	2.1E5	5a	···	0.044
55	30950	204.2578713	−29.8701108	−10.85	2.94	−1.08	0.60	0.08	7.49	2.5E5	5a	···	0.085
56	83925	204.2643496	−29.8439131	−8.71	2.79	−0.97	0.77	0.14	7.44	4.3E4	5a	···	0.129
57	44034	204.2499199	−29.8626794	−9.56	3.10	−0.82	0.44	0.28	6.78	2.1E4	5b	···	0.030
58	17159	204.2616672	−29.8765474	−8.22	3.18	−0.42	0.57	0.16	8.06	4.3E4	5b	···	0.052
59	25716	204.2827697	−29.8725452	−7.28	2.76	−0.14	0.42	0.00	8.41	2.6E4	5b	···	0.054
60	18032	204.2849161	−29.876142	−7.72	2.98	−0.72	0.61	0.36	6.78	5.7E3	5b	···	0.064
61	74692	204.2760088	−29.8475135	−6.99	3.17	−0.04	0.70	0.50	6.74	3.3E3	5b	···	0.075
62	85964	204.2565326	−29.843069	−7.59	2.99	−0.33	0.44	0.00	8.36	2.7E4	5b	···	0.049
63	14748	204.2752747	−29.8776532	−7.14	3.29	−0.11	0.40	0.00	8.36	1.2E4	5b	···	0.038
64	65733	204.2851579	−29.8507302	−9.82	2.73	−0.94	0.61	0.10	7.59	1.3E5	5b	···	0.089
65	65479	204.2862739	−29.8508316	−9.06	3.19	−0.37	0.42	0.00	8.31	7.8E4	5b	···	0.050
66	65304	204.2849235	−29.8508999	−8.51	3.39	0.07	0.80	0.18	8.41	5.8E4	5b	···	0.039
67	10114	204.2664853	−29.8796816	−7.17	2.64	−1.53	−0.33	0.00	6.64	1.4E3	5b	···	0.105
68	58911	204.2807662	−29.8539005	−7.69	2.88	0.15	1.55	0.32	9.11	2.9E5	5b	···	0.050

Table 1—Continued

#	ID	RA	DEC	M_V[a] (mag)	CI[b] (mag)	$U-B$[a] (mag)	$V-I$[a] (mag)	$E(B-V)$ (mag)	Log Age (yr)	Mass (M⊙)	Cat[c]	R(Hα) (pc)	RMS[d]
69	58363	204.2831825	−29.8541717	−7.23	3.27	0.27	0.54	0.00	8.86	2.9E4	5b	···	0.034
70	66553	204.2887134	−29.8504088	−8.06	3.23	0.64	1.08	0.20	9.01	1.5E5	5b	···	0.035
71	55591	204.2710795	−29.8556304	−7.27	3.14	0.34	0.74	0.04	8.86	4.1E4	5b	···	0.036
72	94866	204.2790178	−29.8386224	−8.34	3.28	0.06	0.39	0.00	8.46	4.0E4	5b	···	0.031
73	3113	204.2651882	−29.8828492	−6.93	3.28	0.04	0.89	0.00	9.16	3.8E4	6	···	0.031
74	12505	204.2762954	−29.8786591	−6.67	3.26	0.44	0.97	0.00	9.06	2.2E4	6	···	0.029
75	24528	204.2890323	−29.8730866	−9.15	3.13	−0.14	0.80	0.22	8.36	1.8E5	6	···	0.040
76	55985	204.2695705	−29.8553997	−7.97	2.91	0.02	1.01	0.00	9.26	2.1E5	6	···	0.040
77	18044	204.2956504	−29.8761376	−8.29	3.24	0.12	0.54	0.00	8.61	5.3E4	6	···	0.034
78	54416	204.2898224	−29.8562536	−8.01	3.15	−0.37	0.91	0.38	7.96	6.1E4	6	···	0.042
79	46572	204.2634717	−29.8608741	−8.54	3.05	0.18	0.81	0.04	8.91	1.7E5	6	···	0.058

Note. — [a] Values of M_v throughout this paper assume a distance modulous m - M = 28.28, external extinction Av = 0.229, no correction for internal extinction, and size-dependent aperture corrections described in Chandar et al. (2010). Only external exctinction corrections have been made for values of $U-B$ and $V-I$.

[b] Concentration Index, defined as the magnitude difference between 0.5 and 3 pix radii apertures.

[c] Morphological category as defined in Section 2.

[d] Surface brightness fluctuations measured using the technique described in Section 4. A 4 pixel radius was used for objects 66, 69, 70, 79 rather than the normal 10 pixel radius due to the presence of a likely unrelated bright star within a 10 pixel radius.

[e] The five category 4b clusters with no measured values of Hα are all in the large bubble-like structure below the nucleus of M83 (see Figure 2 in Chandar et al.) 2010. No estimates of R(Hα) are provided for these clusters since the bubble appears to be formed by the integrated effects of a large number of clusters rather than any one individual cluster.

Table 2. Mean Values for Morphological Categories

Category	Mean M_v (mag)	Mean CI (mag)	Mean $E(B-V)$ (mag)	Mean Log Age (yr)	Mean Mass M$\odot$	Mean R(Hα) (pc)	Mean RMS
3	-7.29 ± 1.30	2.56 ± 0.15	0.42 ± 0.10	6.53 ± 0.08	$1.5E4 \pm 3.0E4$	5.0 ± 2.3	0.088 ± 0.021
4a	-8.24 ± 1.29	2.43 ± 0.24	0.17 ± 0.19	6.67 ± 0.09	$1.2E4 \pm 1.4E4$	13.7 ± 5.4	0.125 ± 0.023
4b	-9.63 ± 1.58	2.71 ± 0.29	0.08 ± 0.14	6.79 ± 0.07	$3.6E4 \pm 4.2E4$	38.1 ± 18.5	0.118 ± 0.040
5a	-9.42 ± 0.84	2.90 ± 0.20	0.12 ± 0.10	7.39 ± 0.46	$8.3E4 \pm 8.8E4$	$\cdots$	0.095 ± 0.032
5b	-7.98 ± 0.88	3.08 ± 0.22	0.13 ± 0.16	8.05 ± 0.86	$6.0E4 \pm 7.5E4$	$\cdots$	0.052 ± 0.022
6	-7.94 ± 0.87	3.15 ± 0.13	0.09 ± 0.15	8.76 ± 0.47	$10.4E4 \pm 7.8E4$	$\cdots$	0.039 ± 0.010

Table 3. Parameters for 22 "Single Star" HII Regions

#	ID	RA	Decl.	M_V (mag)	CI (mag)	$U-B$ (mag)	$V-I$ (mag)	R(Hα) (pc)
1	3550	204.2548844	−29.8825632	−5.51	2.13	−1.63	−0.22	9
2	3916	204.2554865	−29.8823689	−5.19	2.30	−1.60	−0.28	8
3	10373	204.2549063	−29.8795771	−5.24	2.28	−1.49	−0.16	7
4	11098	204.2672170	−29.8792752	−6.89	2.02	−1.64	−0.33	14
5	29250	204.2745636	−29.8709998	−4.41	2.09	−1.21	0.02	8
6	35101	204.2745919	−29.8676963	−5.23	2.11	−1.49	−0.39	6
7	37778	204.2667959	−29.8662227	−5.93	2.21	−1.13	0.08	9
8	47544	204.2823703	−29.8602099	−5.86	2.10	−1.51	−0.14	7
9	47772	204.2689918	−29.8600630	−5.09	2.12	−1.31	0.27	7
10	48660	204.2894733	−29.8594131	−4.26	2.25	−1.62	−0.48	2
11	49679	204.2535423	−29.8586761	−5.78	2.18	−0.49	0.32	9
12	50923	204.2552793	−29.8579399	−6.13	2.23	−1.15	0.25	5
13	51301	204.2887045	−29.8577311	−5.19	2.18	−1.27	0.15	2
14	52904	204.2462139	−29.8569822	−4.69	2.23	−1.59	0.14	1
15	56031	204.2828693	−29.8553764	−6.15	2.18	−1.36	0.02	6
16	56485	204.2849019	−29.8551313	−6.19	2.04	−1.42	0.06	8
17	56492	204.2829518	−29.8551272	−6.24	2.24	−0.12	1.07	9
18	56937	204.2841803	−29.8548844	−8.06	2.13	−0.21	0.90	6
19	60624	204.2516243	−29.8530186	−4.99	2.20	−1.28	−0.02	7
20	61345	204.2496746	−29.8526196	−4.79	2.23	−1.25	−0.32	4
21	72114	204.2810230	−29.8485123	−6.34	2.08	−0.77	0.33	12
22	88339	204.2804302	−29.8420518	−4.49	2.30	−1.08	−0.13	7